(d_od_m, 6 H), 7.59 (d_od_m, 6 H). Anal. Calcd for $C_{41}H_{28}$: C, 94.58; H, 5.42. Found: C, 94.60; H, 5.27.

Bis(2-chloro-9-triptycyl)methane (1c). **1c** was similarly obtained in 68% yield and separated into the meso and *dl* isomers by HPLC on a μPorasil column.

***dl* isomer**: mp 395 °C (DSC)[46] (from benzene/hexane); ^{1}H NMR ($CDCl_3$) δ 4.75 (s, 2 H), 5.46 (s, 2 H), 6.68 (t_od_m, 2 H), 6.82–7.13 (m, 8 H), 7.32–7.61 (m, 8 H), 7.63–7.80 (d_od_m + d_m, 4 H). Anal. Calcd for $C_{41}H_{26}Cl_2$: C, 83.53; H, 4.45. Found: C, 83.82; H, 4.34.

Meso isomer: mp 395 °C (DSC)[46] (from benzene/hexane); ^{1}H NMR ($CDCl_3$) δ 4.77 (s, 2 H), 5.47 (s, 2 H), 6.78–7.18 (t_od_m + d_od_m + t_od_m, 10 H), 7.27–7.70 (d_o + d_m + d_od_m + d_od_m, 12 H).

Bis(3-chloro-9-triptycyl)methane (1d). **1d** was similarly obtained from **8d** in 40% yield.

***dl* isomer**: mp 374 °C (DSC)[46] (from benzene/hexane); ^{1}H NMR ($CDCl_3$) δ 4.80 (s, 2 H), 5.45 (s, 2 H), 6.58–7.20 (d_od_m + t_od_m + t_od_m + t_od_m, 10 H), 7.30 (d_o, 2 H), 7.38–7.80 (m, 10 H). Anal. Calcd for $C_{41}H_{26}Cl_2$: C, 83.53; H, 4.45. Found: C, 83.82; H, 4.19.

Meso isomer: mp 374 °C (DSC)[46] (from benzene/hexane); ^{1}H NMR ($CDCl_3$) δ 4.78 (s, 2 H), 5.43 (s, 2 H), 6.64–7.16 (d_od_m + t_od_m + t_od_m, 10 H), 7.27–7.70 (m, 12 H).

Kinetic Measurements. The rates of isomerization were measured in the temperature ranges 200–330 °C for a solution of ethers **2** in diphenylmethane (ca. 2 mg mL^{-1}, ca. 3 mM) and 110–210 °C for a solution of methanes **1** in *o*-dichlorobenzene. At each temperature, small glass ampules (ca. 2-mm i.d. and 4-cm long) containing the solution were immersed in a refluxing solvent (>100 mL). After a given period of time (a few minutes to several days), they were taken out of the bath and cooled in ice–water to stop the isomerization reaction. In order to obtain the *dl*/meso ratios at infinite time, they were subjected to continued heating for at least several half-lives in the temperature range of fairly rapid isomerization. When isomerization was very slow, the sample solution was first equilibrated at higher temperatures and then maintained at the given temperature for a few half-lives.

Analysis of the rate data was carried out according to eq 3 and 4,

$$\text{meso} \underset{k}{\overset{kK}{\rightleftharpoons}} dl \tag{3}$$

$$k(K + 1)t = \ln (x_\infty(1 + x/\epsilon)/(s_\infty - x)) \tag{4}$$

where k, K, $\epsilon = \epsilon_{dl}/\epsilon_{meso}$, and $x = A_{dl}/A_{meso}$ are the rate constants for isomerization from the *dl* to meso isomers, the equilibrium constant defined as C_{dl}/C_{meso}, the ratio of molar absorptivitiy at 254 nm, and the observed ratio of absorbance of the two isomers at the same wavelength, respectively. The experimentally determined ε's were in the range 1.00–1.03. Since the right-hand side of eq 4 is rather insensitive to ϵ near $\epsilon \simeq 1.00$, the ϵ values were assumed to be unity. Equation 4 now reduces to eq

$$k(K + 1)t = \ln (x_\infty(1 + x)/(x_\infty - x)) \tag{4'}$$

The solvents and chemicals used for the constant-temperature bath were as follows: anthracene (344 °C), nonadecane (333 °C), octadecane (319 °C), heptadecane (305 °C), bibenzyl (286 °C), biphenyl (258 °C), tridecane (238 °C), 1,2,4-trichlorobenzene (217 °C), undecane (197.1 °C), *o*-dichlorobenzene (181.0 °C), mesitylene (167.2 °C), 1,1,2,2-tetrachloroethane (150.0 °C), chlorobenzene (132.9 °C), and toluene (112.7 °C). The temperatures given above are slightly but not greater than a few degrees higher than the reported boiling points of these chemicals, since both the samples for the kinetic measurements and a thermocouple (chromel–alumel for ≥200 °C and copper–constantan for <200 °C) were directly immersed in the liquid. The temperature reading is considered to be accurate to ±1 and ±0.3 °C above and below 200 °C, respectively.

Analyses of the isomer ratios were carried out by an HPLC instrument equipped with a Shimadzu CR 1-A data processor.

Acknowledgment. We are grateful to Professor Yonezo Morino for valuable comments and encouragements. We would also like to thank Professor Kurt Mislow for helpful comments on our previous papers of the series and for providing a copy of his manuscripts prior to publication.

Registry No. 1a, 73611-46-8; *dl*-**1c**, 84065-14-5; *meso*-**1c**, 84065-15-6; *dl*-**1d**, 84065-16-7; *meso*-**1d**, 84065-17-8; **2a**, 73611-45-7; **2b**, 84065-18-9; *dl*-**2c**, 84065-19-0; *meso*-**2c**, 84065-20-3; *dl*-**2d**, 78150-15-9; *meso*-**2d**, 78129-63-2; **3c**, 84065-21-4; **3d**, 84065-22-5; **4a**, 15364-55-3; **4b**, 84065-23-6; **4b**, 84065-24-7; **4c**, 78129-64-3; **4d**, 78129-59-6; **5c**, 23716-41-8; **5d**, 84065-25-8; **6c**, 84065-26-9; **6d**, 84065-27-0; **7c**, 84065-28-1; **7d**, 84065-29-2; **8a**, 15080-14-5; **8c**, 84065-30-5; **8d**, 84065-31-6; **10b**, 84065-32-7; **10c**, 84065-33-8; **10d**, 78129-60-9; **11a**, 73597-15-6; **11b**, 84065-34-9; **11c**, 84065-35-0; **11d**, 78129-62-1; **12a**, 73597-17-8; 2-chloroanthracene, 17135-78-3; 9-bromoanthracene, 1564-64-3; anthranilic acid, 118-92-3; 2-amino-3-methylbenzoic acid, 4389-45-1; 1-methyltriptycene, 20711-97-1; 4-methyl-9-hydroxytriptycene, 84065-36-1; 2-chloro-9-hydroxytriptycene, 84065-37-2; 2-chlorotriptycene, 20711-99-3; 2-chloro-9,10-dibromoanthracene, 84065-38-3.

(46) The apparently identical melting point was obtained either for the meso or *dl* isomers of the methanes, showing the isomerization in the solid state during DSC (see text).

MCSCF/CI Investigation of the Low-Lying Potential Energy Surfaces of the Formyloxyl Radical, HCO_2·

David Feller, Earl S. Huyser,† Weston Thatcher Borden, and Ernest R. Davidson*

Contribution from the Department of Chemistry BG-10, University of Washington, Seattle, Washington 98195. *Received August 26, 1982*

Abstract: Configuration interaction calculations have been performed on the low-lying potential energy surfaces of the formyloxyl radical. Minima and transition-state geometries were determined by an MCSCF procedure. The energies were then refined by large CI calculations. These calculations show the radical to have a σ ground state and a low-energy π excited state. On the ground-state surface, the lowest C_{2v} $^2B_2$ and $^2A_1$ energies are connected by a low-energy path passing through $^2A'$ points with unequal C–O bond lengths. This surface contacts the second $^2A'$ surface at the $^2B_2$–$^2A_1$ crossing point to form a Jahn–Teller double cone. On the lowest surface for a π radical, a C_{2v} $^2A_2$ energy is found to be a minimum, but there is very little energy change for large-amplitude asymmetric stretching. The transition states for fragmentation of HCO_2· to H· + CO_2 and for rearrangement to ·CO_2H have also been determined.

Introduction

As a prototype acyloxyl radical, HCO_2· has been the subject of several recent theoretical investigations that have dealt with the three lowest energy states. These states are obtained by singly occupying one of the energetically similar $6a_1$, $4b_2$, and $1a_2$ oxygen lone-pair orbitals, which are respectively the in-phase and out-of-phase combinations of oxygen nonbonding σ orbitals and the out-of-phase combination of oxygen π orbitals. We find that the corresponding orbital energies in the HCO_2^- anion, in which all

†Permanent Address: Department of Chemistry, University of Kansas, Lawrence, Kans. 66045.

0002-7863/83/1505-1459$01.50/0

three orbitals are doubly occupied, fall within 50 mhartrees of each other at an OCO bond angle of 114°. Because of the proximity in energy of these three states of HCO_2·, past theoretical results have differed in their conclusions concerning the order of these states and the geometry of the molecule.

Unpublished, minimal basis set, unrestricted Hartree–Fock (UHF) calculations by Newton are quoted by Karch et al.[1] as indicating a $^2A_2$ π ground state for the formyloxyl radical. Kikuchi[2] has published open-shell restricted Hartree–Fock (RHF) calculations at symmetric (C_{2v}) and planar nonsymmetric geometries that were estimated from semiempirical work. His results suggested a nonsymmetric σ ground state. Subsequent multiconfiguration SCF (MCSCF) geometry optimizations with the semiemprical MINDO/3 method showed the σ state to be symmetric ($^2B_2$) and 2.2 kcal/mol lower than the π state.[3] Spin-unrestricted MNDO calculations on HCO_2· by Dewar, Pakiari, and Pierini[4] yielded a nonsymmetric σ minimum, 4.3 kcal/mol below the symmetric π minimum. Dewar et al. noted that, because MNDO tends to overestimate the relative stability of π radicals, the actual σ–π gap may be larger.

Minimal basis set configuration interaction (CI) calculations by Baird and Taylor[5] showed a small (2.8 kcal/mol) energy difference between the lowest σ and π states, with π state lower. With the exception of the CH bond length, geometries were optimized at the CI level of theory. Subsequent CI calculations at these same geometries using the larger 4-31G basis produced an even smaller (1.4 kcal/mol) separation, with the π state still lower. While the π state was found to favor a C_{2v} geometry, the σ state of HCO_2· showed the greatest asymmetry in C–O bond lengths (1.41 vs. 1.25 Å for the two C–O bonds) of any of the radicals considered in the study. The CI calculations done by Baird and Taylor involved all single, double, and triple excitations among three π and two σ orbitals.

Very recently, Peyerimhoff, Skell, May, and Buenker[6] performed large basis set, multireference, double excitation, CI calculations on the formyloxyl and acetoxyl (CH_3CO_2·) radicals at C_{2v} geometries. Their estimated full CI energies for the former radical show the $^2B_2$ (σ) energy to lie 7.2 kcal/mol below the $^2A_1$ (σ) energy and 13.7 kcal/mol below the $^2A_2$ (π) energy. A close correspondence between the ordering of the electronic states of the two radicals was found. Peyerimhoff et al. made some effort to determine whether their C_{2v} geometries were true minima by performing CI calculations at geometries obtained by simultaneously lengthening one CO bond while shortening the other by the same fixed amounts (0.113 and 0.226 Å). No decrease in energy was found at the $^2A_2$ (π) geometry. However, at the crossing point of the C_{2v} OCO bending curves for the σ wave functions, the energy was found to decrease slightly on this type of bond-length change.

Experimentally, EPR studies by McBride and Merrill[7] on the benzoyloxyl radical, $C_6H_5CO_2$·, suggest a σ ground state with C_{2v} symmetry ($^2B_2$). The results of EPR studies on other acyloxyl radicals have been interpreted by McBride and Merrill as being consistent with this assignment. Based on results in chain reactions involving acyloxyl radicals, Skell and May[8] have suggested that both σ and π states are accessible and that the state populated depends on the mode by which the radicals are generated.

The goals of the ab initio study of formyloxyl reported here were threefold: to determine the preferred geometries of the low-lying electronic states, to compute their relative energies, and to find the transition states for possible reactions on the ground-state potential surface, particularly for the fragmentation to H· + CO_2.

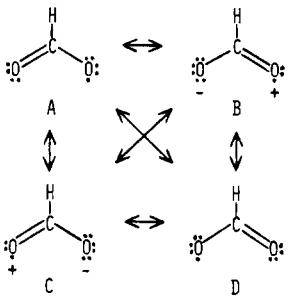

Figure 1. Resonance structure for states of formyloxyl in which the unpaired electron occupies a σ MO. σ or π electron delocalization leads to ionic terms (represented by structures B and C) in the wave function, unless the motions of the σ and π electrons are correlated (as in A ↔ D).

Procedure and Results

The present calculations utilized moderately large MCSCF wave functions (539–2205 spin-adapted configurations, depending on the symmetry) with split valence plus polarization (SVP) basis sets containing one set of d functions on carbon and oxygen. The MCSCF calculations were followed by larger basis set, extensive CI's at all stationary points to help refine relative energy differences and to obtain molecular properties. The MCSCF calculations were performed with a recent version of GAMESS,[9] an analytical gradient MCSCF program from NRCC. The CI wave functions and properties were obtained with MELD, a group of programs written in this laboratory.

In spite of the dominance of the HF configuration in CI expansions of the states of interest in formyloxyl, any single configuration description of the π radical will be plagued by the so-called "doublet instability" phenomenon. This phenomenon is characterized by broken symmetry solutions of the restricted HF equations at symmetric geometries, with a concomitant prediction of unequal bond lengths. In three-center radicals containing three π electrons, an RHF calculation tends to localize the odd electron at one end of the molecule, while localizing a double bond at the other end. This spurious localization compensates for the inadequacy of the HF single configuration in providing correlation of the two opposite-spin π electrons.

The "doublet instability" effect has been extensively studied in the case of the allyl radical, CH_2CHCH_2, a molecule isoelectronic with formyloxyl. Work by Paldus and Veillard[10] showed that, in allyl, the magnitude of the energy lowering that accompanies RHF symmetry breaking is inversely correlated with the size of the basis set. They found the biggest effect with a minimal basis set. With a much larger basis and optimized geometries, the energy lowering on symmetry breaking was reduced to less than a microhartree. However, even for fixed bond lengths, improvement of the basis set decreased the energy lowering.

Unlike the case in allyl, we find that the π state of formyloxyl shows a slight increase in the energy difference between the symmetric and broken symmetry RHF energies upon basis set enlargement. RHF calculations with the STO-3G[11] basis (at the $^2A_2$ C_{2v} SVP–MCSCF geometry) yielded an energy for the broken symmetry wave function 0.0067 hartree lower than the C_{2v} constrained result. Similar calculations with the Dunning[12] double-ζ polarization (DZP) basis set at the same C_{2v} geometry showed a difference of 0.0084 hartree.

The work of Kikuchi[3] as well as that of Baird and Taylor[5] suggested that correlating the motions of the three π electrons would result in a single C_{2v} minimum and a symmetric wave

(1) Karch, N. J.; Koh, E. T.; Whitsel, B. L.; McBride, J. M. *J. Am. Chem. Soc.* **1975**, *97*, 6729.
(2) Kikuchi, O. *Tetrahedron Lett.* **1977**, *28*, 2421.
(3) Kikuchi, O. *Bull. Chem. Jpn.* **1980**, *53*, 3149.
(4) Dewar, M. J. S.; Parker; A. H.; Pierini, A. B. *J. Am. Chem. Soc.* **1982**, *104*, 3242.
(5) Baird, N. C.; Taylor, K. F. *Can. J. Chem.* **1980**, *58*, 733.
(6) Peyerimhoff, S. D.; Skell, P. S.; May, D. D.; Buenker, R. J. *J. Am. Chem. Soc.* **1982**, *104*, 4515.
(7) McBride, J. M.; Merrill, R. A. *J. Am. Chem. Soc.* **1980**, *102*, 1723.
(8) Skell, P. S.; May, D. D. *J. Am. Chem. Soc.* **1981**, *103*, 967; *Ibid.* **1982**, *104*, 4500.
(9) Dupuis, M.; Spangler, D.; Wendoloski, J. J. NRCC Software Catalog, Vol. 1, Program GG01 (GAMESS), 1980.
(10) Paldus, J.; Veillard, A. *Mol. Phys.* **1978**, *35*, 445.
(11) Hehre, W. J.; Stewart, R. F.; Pople, J. A. *J. Chem. Phys.* **1969**, *51*, 2657.
(12) Dunning, T. H., Jr. *J. Chem. Phys.* **1970**, *53*, 2823.

function for the π state of formyloxyl. Takada and Dupuis[13] have shown that three-orbital/three-electron full π-space MCSCF produces a single minimum on the ground-state potential surface of allyl, in accord with EPR results. Thus, as anticipated, our 3-21G[14] MCSCF calculations, involving all possible arrangements of the three π electrons among the three π molecular orbitals available in the conceptual minimal basis set space, showed the existence of only one minimum, possessing C_{2v} symmetry, for the lowest π state of formyloxyl.

Previous calculations reported mixed conclusions[1-6] regarding the energy ordering of the π and σ states. We also find the state ordering to be very sensitive to basis set and electron correlation effects. For instance, our best RHF results show that the π state is clearly lowest at the C_{2v} constrained RHF level of calculation. At C_{2v} geometries, however, electron correlation is even more important for the σ states of formyloxyl than it is for the π state. In the σ states it is essential to correlate the σ lone pair that occupies $6a_1$ in $^2B_2$ or $4b_2$ in $^2A_1$ with the π lone pair in $1a_2$. Otherwise, as shown in Figure 1, the wave functions contain high-energy ionic terms corresponding to simultaneous appearance of these lone pairs on the same oxygen atom. When this σ–π correlation is included, the σ state is predicted to be the ground state.

At nonsymmetric geometries the RHF result already places the σ state lower than π, because the RHF wave function obtained for the σ state automatically includes much of the σ–π correlation effect. In this wave function the σ lone pair is localized on one oxygen and the π lone pair is localized on the other. Consequently, this type of localized RHF wave function is preferred for symmetrical geometries too. This effect causes an even larger symmetry instability than that discussed above for the π state. At the $^2B_2$ C_{2v} SVP-MCSCF geometry the RHF energy with the DZP basis is lowered by 0.0307 hartree upon allowing the wave function to have less than C_{2v} symmetry. Hence, even greater care is required in the σ states than in the π to ensure a smooth connection between energies computed at symmetric and nonsymmetric geometries.

Since one of the goals of this work was the study of the dissociation of hydrogen from the σ state, it was also necessary to correlate the electrons in the C–H bond. Therefore, the set of orbitals among which excitations were permitted was expanded to include four σ orbitals, as well as the original three π orbitals. The number of σ orbitals was arrived at by considering the CO_2 + H· dissociation asymptotes. In that region of the potential surface it was desirable to include, in addition to the H orbital, the three in-plane π orbitals of CO_2, in order to balance the 3 out-of-plane π orbitals. These seven-orbital/nine-electron full MCSCF calculations involved 242 configurations in C_{2v} symmetry.

Unfortunately, the active σ orbitals produced by this MCSCF calculation at the $^2B_2$ geometry did not include the CH bonding and antibonding orbitals, as is necessary if the wave function is to go smoothly from the HCO_2· region to the CO_2 + H· region. However, a further enlargement of the MCSCF "active space" was successful in including the desired orbitals. Thus, the final choice of active orbitals involved eight of σ symmetry (five SCF-occupied correlated by three virtuals) and three of π symmetry. MCSCF calculations with this set of active orbitals will be referred to as 11-orbital/13-electron calculations. Orbital contour plots of the eight active σ MCSCF natural orbitals for the $^2B_2$ state are included in Figure 2. Unlike the seven-orbital/nine-electron calculations, for which it was possible to include all configurations consistent with the point group symmetry and multiplicity, the larger 11 orbital active space required restricting the configuration list to those having no more than two electrons outside the SCF-occupied orbital set (RE-MCSCF). Convergence of the calculations was significantly slower than with the seven-orbital/nine-electron full MCSCF. Therefore, total energies were only converged to about 10 μhartrees, except at points for which

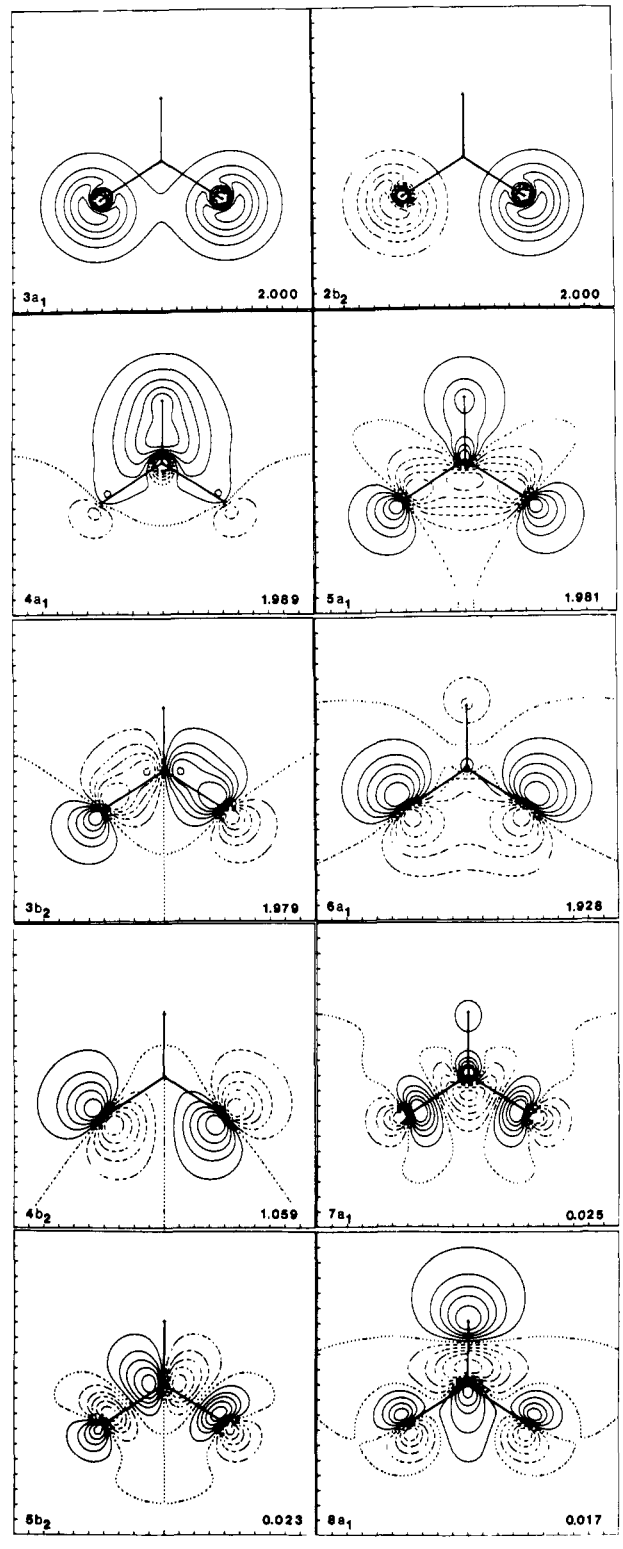

Figure 2. The eight active and two lower energy inactive MCSCF σ natural orbitals for the $^2B_2$ state. Orbital contours enclose 90, 70, 50, 30, and 10% of the probability density. Occupation numbers are given in the lower right hand of each square. The three π orbitals are not shown.

normal mode vibrational analyses were desired. Here the energies were converged to 1 μhartree. Geometry optimizations were stopped when the largest component of the gradient was less than 0.003 hartree/bohr. This corresponds to an uncertainty of about 0.005 Å in bond lengths and 1.0° in bond angles.

An unexpected result of the seven-orbital/nine-electron calculations was the prediction of a minimum energy geometry on the π state surface with unequal C–O bond lengths. This $^2A''$

(13) Takada, T.; Dupuis, M., private communication.
(14) Binkley, J. S.; Pople, J. A.; Hehre, W. J. *J. Am. Chem. Soc.* **1980**, *102*, 939.

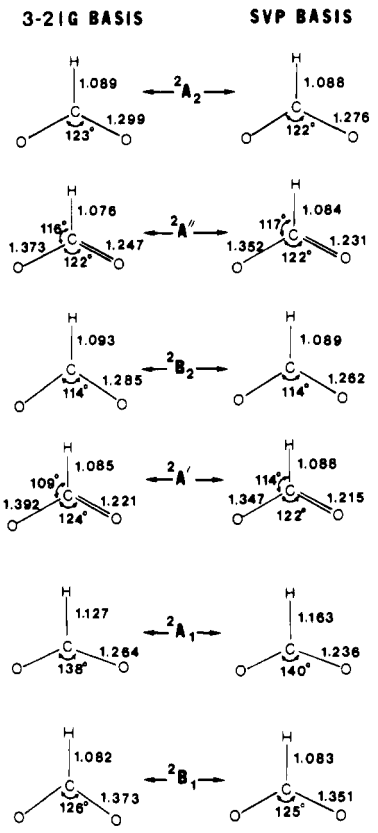

Figure 3. Optimal and transition state 11-orbital/13-electron MCSCF geometries with the 3-21G and SVP basis sets. Bond lengths are in ångströms.

minimum was 0.0023 hartree lower than the π minimum which possessed C_{2v} symmetry ($^2A_2$). This finding contrasts with the π space MCSCF results, which showed an energy minimum only at the C_{2v} geometry.

Subsequent 11-orbital/13-electron RE-MCSCF results with the same 3-21G basis also found an A'' minimum. A normal mode vibrational analysis showed the optimal C_{2v} constrained geometry to be a true minimum on the potential surface too, with a low frequency mode (600.1 cm^{-1}) corresponding to asymmetric C–O stretch. The transition state connecting the C_{2v} and C_s minima was not determined in detail. Instead, a sequence of points was computed along a linearly interpolated pathway in the internal coordinate space of the π radical. The maximum along this linear synchronous transit (LST)[15] pathway occured at a point approximately 20% of the way from the C_{2v} to the C_s minimum and had an energy 0.4 kcal/mol above the C_{2v} minimum. The surface is flat enough between the C_{2v} and C_s minima that the nature of these points could easily change with a larger polarized basis set or with a greater number of configurations. A vibrational analysis with such an improved wave function was not attempted because it would have been prohibitively expensive. The optimal MCSCF geometries for the $^2A_2$ and $^2A''$ energy minima with the 3-21G basis are shown in Figure 3. Total energies are given in Table I.

Optimal MCSCF geometries were also determined for stationary points on the potential surface for the σ radical. The geometries are given in Figure 3, while the corresponding energies are listed in Table I. A schematic representation of the HCO_2· portion of the MCSCF potential surface is shown in Figure 4. The depth of the nonsymmetric minima on the σ and π surfaces is exaggerated to emphasize their presence. In an effort to keep the diagram from becoming too complicated, the mirror image $^2A'$ σ and $^2A''$ π minima are not shown.

The σ surfaces in Figure 4 appear considerably more complicated than the π surface, although the optimum nonsymmetric

Table I. MCSCF Energies at Stationary Points Obtained with the 3-21G Basis

HCO_2	wave function	config[a]	type[c]	energy
		π-State Energies		
$^2A_2$	3-orb/3-el full MCSCF	4	min	−187.1061
$^2A_2$	7-orb/9-el full MCSCF	30	min	−187.1429
$^2A''$		242	min	−187.1464
$^2A_2$	11-orb/13-el RE MCSCF	539	min	−187.2014 (0.5)[b]
$^2A''$		1076	min	−187.2028 (−0.4)
$^2B_1$		537	min	−187.0650 (86.1)
		σ-State Energies		
$^2B_2$	11-orb/13-el RE MCSCF	562	SP	−187.2022 (0.0)
$^2A'$		1129	min	−187.2140 (−7.4)
$^2A_1$		567	SP	−187.1943 (5.0)
$^2A_1$		567	TS	−187.1875 (9.2)
CO_2 + H· ·CO_2H		325	min	−187.2308 (−17.9)
$^2A'$ (trans)		1129	min	−187.2198 (−11.0)
$^2A'$		1129	TS	−187.1472 (34.5)

[a] The number of spin-adapted configurations involved in the MCSCF calculation. [b] Energy differences with respect to the $^2B_2$ state in kcal/mol. [c] SP is the saddle point for pseudorotation; TS is the transition state for reactions.

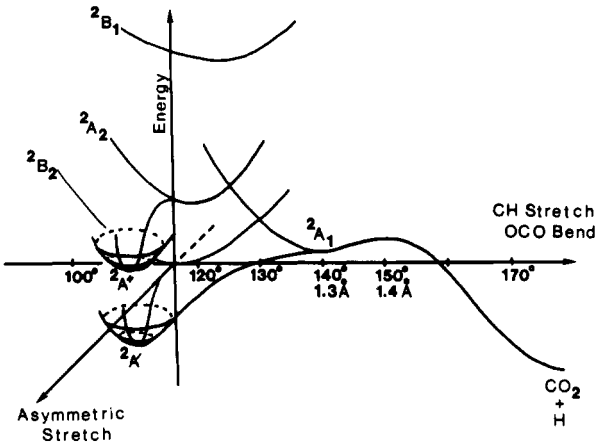

Figure 4. A schematic representation of the HCO_2· portion of the MCSCF potential surfaces.

σ and π geometries are quite similar. The σ surfaces are best described as forming a Jahn–Teller double cone with many features reminiscent of the similar surfaces previously reported for NO_2.[16] At C_{2v} geometries with small bond angles, the $^2B_2$ energy is the lowest. In this state the O–O antibonding $4b_2$ orbital is singly occupied. The optimum $^2B_2$ OCO bond angle (114°) is somewhat greater than the value (104°) found in the same state of NO_2. For C_{2v} geometries with larger bond angles, repulsive through-bond interactions in $6a_1$ dominate the repulsive through-space interactions in $4b_2$. The $^2A_1$ state is lower in energy because, in this state, the $4b_2$ MO is doubly occupied, and only one electron occupies $6a_1$. The $^2A_1$ bond angle is 138° in HCO_2· and 133° in NO_2. Because the $6a_1$ orbital in the $^2A_1$ state of formyloxyl has a large coefficient on carbon and hydrogen, the $^2A_1$ state of formyloxyl has a high spin density on these two atoms. In addition, since $6a_1$ contributes to C–H bonding at large bond angles, the C–H bond is quite long (1.163 Å with the SVP basis set) in $^2A_1$, where this MO is only singly occupied.

The crossing of the $^2A_1$ and $^2B_2$ potential surgaces at intermediate OCO bond angles gives rise to a Jahn–Teller double cone for molecular distortions that allow these C_{2v} wave functions to mix. A force constant analysis with the 3-21G basis, 11-orbit-

(15) Halgren, T. A.; Lipscomb, W. N. *Chem. Phys. Lett.* **1977**, *49*, 225.

(16) Jackels, C. F.; Davidson, E. R. *J. Chem. Phys.* **1976**, *65*, 2941.

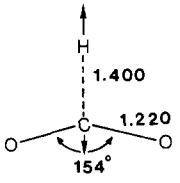

Figure 5. The transition state for loss of hydrogen from $^2A_1$. Arrows indicate the major components of the reaction coordinate.

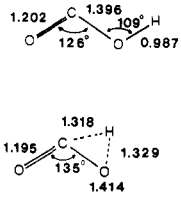

Figure 6. Optimal and transition state 11-orbital/13-electron MCSCF geometries obtained with the 3-21 basis for $\cdot CO_2H$.

al/13-electron MCSCF wave function showed that both the $^2A_1$ and $^2B_2$ C_{2v} stationary points have a negative force constant for asymmetric stretch. Hence, they both connect smoothly via pseudorotation to the mirror image pair of A′ minima, whose bond angle of 123° is near that at the apex of the cone where $^2A_1$ and $^2B_2$ cross.

The π surface must actually have some complications which have not been explored. As shown in Figure 4, the π surface has an energy between the upper and lower surfaces of the $^2A'$ double cone at the $^2A_1$, $^2B_2$, and $^2A'$ stationary points on the lower π state surface. One must therefore expect an additional complication due to the interaction of the σ and π surfaces, which will lead to mixing of these states under out-of-plane motion of the proton. This coupling matrix element should be small, however, and probably would not lead to nonplanar minima. Nevertheless, the coupling does provide a radiationless path from the $^2A''$ π to the $^2A'$ σ surfaces. Since the π state is about the same energy as the calculated transition state on the σ surface for going to CO_2 + H·, the π state might dissociate easily.

Dissociation of formyloxyl to CO_2 + H· on the ground $^2A'$ state σ potential surface is an interesting process. The lowest energy path starting from the $^2A'$ minimum is a pseudorotation (increasing the OCO bond angle and CH bond length while decreasing the CO bond length asymmetry) to the $^2A_1$ saddle point. From there, a further increase in bond angle and CH bond length leads to the transition state for CH bond breaking. At this transition state we have verified that there is only one negative force constant, corresponding largely to CH stretch. Thus, somewhere along the path connecting the $^2A_1$ saddle point and the transition state for loss of hydrogen (also $^2A_1$), the force constant for asymmetric stretch reverses sign, and the path becomes stable to asymmetric CO bond length distortions.

As shown in Figure 5, at the transition state the OCO angle is 154°, and the C–H bond is 1.40 Å. The large OCO bond angle and long C–H bond at the $^2A_1$ saddle point for pseudorotation suggest that loss of hydrogen from this point on the lowest A′ σ surface should proceed with only a small barrier. Indeed, as shown in Table I, the transition state for loss of hydrogen was found to be only 4.2 kcal/mol higher than $^2A_1$, while the dissociated products (CO_2 + H·) lie 22.9 kcal/mol lower than $^2A_1$.

Besides undergoing loss of hydrogen, the σ radical can undergo a 1,2-hydrogen shift in which hydrogen migrates from carbon to the singly bonded oxygen. MCSCF geometry optimization with the 3-21G basis shows the resulting trans form of $\cdot CO_2H$ to be lower in energy than any $HCO_2\cdot$ structure. The optimal geometry and total energy are given in Figure 6 and Table I, respectively. A SD-CI calculation with the DZP basis was performed at a geometry derived from the 3-21G geometry by shortening the CO bonds by 0.02 Å in order to approximate the effect of MCSCF geometry optimization with a polarized basis set (vide infra). At the CI level of theory this form of the radical is approximately 2 kcal/mol lower in energy than CO_2 + H·.

Table II. 11-Orbital/13-Electron MCSCF Energies with the SVP Basis

	state	energy	state	energy
$HCO_2\cdot$	$^2A_2$	−188.2853 (6.2)[a]	$^2A''$	−188.2866 (5.4)
	$^2B_2$	−188.2952 (0.0)	$^2A'$	−188.3029 (−4.8)
	$^2A_1$	−188.2842 (6.9)	$^2B_1$	−188.1496 (91.4)
CO_2 + H·		−188.3290 (−21.2)		

[a] Energy difference with respect to the $^2B_2$ state in kcal/mol.

The transition state leading to the trans form of $\cdot CO_2H$ was also located with the 3-21G basis. It is shown in Figure 6, and its energy is listed in Table I. The transition state is 41.9 kcal/mol above the $^2A'$ and 45.5 kcal/mol above the trans form of $\cdot CO_2H$ at the MCSCF level of theory. With the DZP basis, CI predicts a slightly smaller 38.9 kcal/mol barrier to go from $^2A'$ to $\cdot CO_2H$. Hence, the lowest energy pathway for this rearrangemenet would probably be loss of hydrogen from carbon, followed by readdition to oxygen, rather than concerted hydrogen migration. This conclusion is in agreement with the results of Harding on 1,2-hydrogen shifts in other radicals.[17]

The geometries of the six states shown in Figure 3 were reoptimized with the larger Dunning[18] [3s,2p,1d/2s] split valence polarization basis (SVP). The SVP geometries are shown in Figure 2 alongside the corresponding small basis set results. Although bond angles are essentially unchanged, C–O bond lengths are decreased by an average of 0.023 Å. The C–O bond length in CO_2 is 1.167 Å with this basis, compared to 1.181 Å with 3-21G. These geometries are in agreement with the MRD-CI geometries of Peyerimhoff et al., except for the CH bond length for $^2A_1$, for which they used a fixed value of 1.085 Å.

The inclusion of d-type polarization functions on carbon and oxygen was shown to be energetically important for formyloxyl by the work of Peyerimhoff et al. As seen in Table II and Figure 7, the σ states are preferentially stabilized relative to the π states by the polarized basis set. Both the lowest σ and π states are still predicted to prefer geometries with unequal CO bond lengths at this level of theory. The energy difference between the C_s and C_{2v} geometries has decreased from 7.4 to 4.8 kcal/mol for the σ state.

Additional effects of electron correlation were investigated by performing a set of multireference single and double excitation CI's (SD-CI) at the optimal SVP basis set MCSCF geometries. These calculations utilized the Dunning [4s,2p,1d] contracted basis set on carbon (d exponent = 0.75) and oxygen (d exponent = 0.85) and a [3s,1p] contracted basis on hydrogen (p exponent = 1.0) for a total of 54 basis functions. We shall refer to this as the double ζ polarization (DZP) basis set. The occupied SCF orbitals were determined for symmetry-constrained parent-configuration wave functions for each state at each geometry.

The large number of double excitations (more than 1.8×10^6 in some cases) made it necessary to perform variational calculations on a subset of the full SD-CI configuration space. Therefore, it was desirable to recover a large percentage of the SD-CI correlation energy with as few configurations as possible. Although an extrapolation based on the second-order perturbation theory estimate of the neglected correlation energy can be made, the accuracy of the extrapolation improves with the percentage of energy variationally recovered. K orbitals have been shown to be an efficient way to mimic the frozen natural orbital set for many closed- and open-shell molecules. Hence, the transformation of the virtual space to K orbitals[19] was made in order to improve the convergence of the CI.

Tests of the quality of these orbitals were made with the SVP basis on the lowest σ state of the radical. Using the same configuration list as was previously used in the MCSCF calculations, K-orbital CI's recovered 75% of the MCSCF correlation energy. However, while MCSCF orbitals are optimal for excitations among

(17) Harding, L. B. *J. Am. Chem. Soc.* **1981**, *103*, 7469.
(18) Dunning, T. H., Jr.; Hay, P. J. In "Modern Theoretical Chemistry" Schaefer, H. F., III, Ed.; Plenum Press: New York, 1977; Vol. 2.
(19) Feller, D.; Davidson, E. R. *J. Chem. Phys.* **1981**, *74*, 3877.

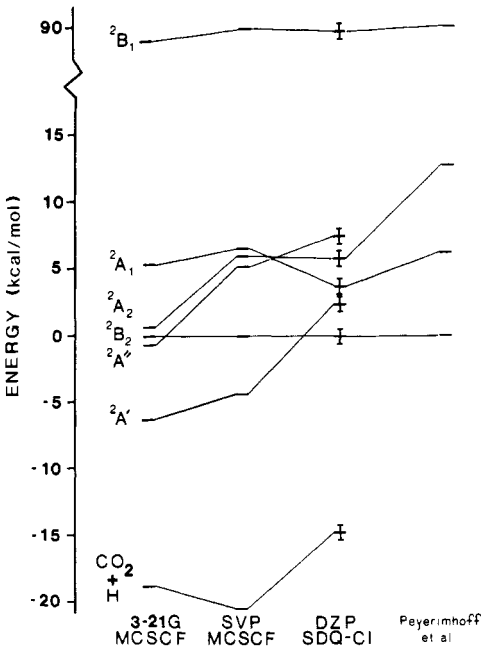

Figure 7. Relative energies obtained with various basis sets and different types of wave functions.

Table III. Convergence of the Estimated SDQ-CI Energy[a]

size ref space	size full SD	size selected CI	% corr[b]	E(SDQ-CI)
1	40 983	12 171	85	−188.615
3	142 921	13 703	86	−188.626
4	182 162	15 425	87	−188.624
6	255 508	15 552	87	−188.625
14	349 775	15 731	87	−188.626

[a] DZP basis for $^2B_2$ state at SVP-MCSCF $^2B_2$ geometry. Threshold = 10^{-5} hartree. [b] Percentage of correlation energy recovered variationally by selected CI, relative to E(SDQ-CI) − E(SCF), where E(SDQ-CI) = −188.626 hartrees and E(SCF) = −188.123 hartrees.

the active space orbitals, most of the configurations in large-scale multireference SD-CI involve orbitals outside the active space.

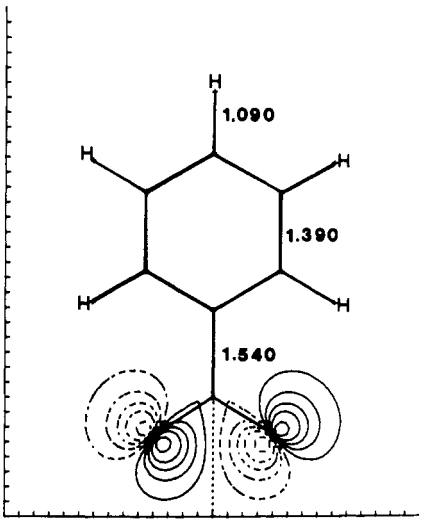

Figure 8. The $11b_2$ SCF orbital for the $^2B_2$ state of the benzoyloxyl radical.

These orbitals are defined by the MCSCF procedure only to the extent that they are orthogonal to the occupied orbitals; thus, they should not be particularly good for correlation purposes. K orbitals, on the other hand, define the entire SCF virtual space.

Configurations were selected for inclusion in the CI based on their estimated energy contribution. The quantity of energy ignored by excluding some of the configurations was estimated by scaling the perturbation theory estimate of this quantity by the ratio of the actual CI energy lowering to the predicted lowering by the configurations kept. Typically 90–95% of the estimated total SD-CI correlation energy was variationally recovered. Tests on this molecule indicated that errors on the order of 1–2 mhartrees could be expected in the extrapolated SD-CI energy at this level of calculation.

In order to determine what configurations should be included in the reference wave function, from which single and double excitations were considered, CI calculations were performed with a sequence of successively larger reference spaces. A correction was made for higher order excitations[20] which are far too numerous

Table IV. DZP-SCF and CI Energies at the SVP MCSCF Geometries

C_{2v} Constrained Wave Functions

state	$^2B_2$		$^2A_2$		$^2A_1$	
geometry	E(SCF)	E(SDQ-CI)	E(SCF)	E(SDQ-CI)	E(SCF)	E(SDQ-CI)
$^2B_2$	−188.122 9	−188.626	−188.122 9	−188.599	−188.064 6	−188.579
$^2A_2$	−188.113 1	−188.620	−188.123 9	−188.617	−188.083 1	−188.599
$^2A_1$	−188.082 2	−188.589			−188.111 2	−188.620

state	$^2B_1$		$^2A_1$ (TS)	
geometry	E(SCF)	E(SDQ-CI)	E(SCF)	E(SDQ-CI)
$^2B_2$	−187.940 7	−188.462		
$^2A_2$	−187.954 3	−188.475		
$^2B_1$	−187.948 5	−188.483		
$^2A_1$	(TS)		−188.112 0	−188.610

C_s Constrained Wave Functions

state	$1^2A'$		$2^2A'$		$^2A''$	
geometry	E(SCF)	E(SDQ-CI)	E(SDQ-CI)	geometry	E(SCF)	E(SDQ-CI)
$^2A'$	−188.169 5	−188.622	−188.607	$^2A''$	−188.146 7	−188.613
$^2B_2$	−188.153 6			$^2A_2$	−188.132 3	

Miscellaneous Geometries

geometry		E(SCF)	E(SDQ-CI)	geometry	E(SCF)	E(SDQ-CI)
$\cdot CO_2H$ (trans)	$^2A'$	−188.170 7	−188.650	CO_2 + H·	−188.174 7	−188.647
$\cdot CO_2H$ (cis)	$^2A'$	−188.175 9	−188.658	CO + OH·	−188.166 1	−188.617
$\cdot CO_2H$ (TS)	$^2A'$	−188.067 9	−188.568			

Table V. Selected Molecular Properties Obtained with the SD-CI Wave Functions

	state				
	$^2B_2$	$^2A_2$	$^2A_1$	$^2A'$	$^2A''$
y dipole (D)	0.0	0.0	0.0	−1.280	−0.590
z dipole (D)[a]	2.716	1.888	1.971	2.294	2.038
			Carbon		
field gradient[b]					
$q(yy)$ (au)	−0.1266	−0.0425	−0.2257	−0.0049	−0.0037
$q(zz)$ (au)	−0.3706	−0.3100	−0.1692	−0.4016	−0.3664
$\theta(zz)$ (deg)	0.0	0.0	0.0	22.8	18.0
anisotropic hyperfine					
$A(yy)$ (au)	0.0599	0.1229	0.0314	0.0650	0.0913
$A(zz)$ (au)	0.0085	0.0392	0.0503	−0.0170	0.0008
$\theta(zz)$ (deg)	0.0	0.0	0.0	24.7	18.2
			Oxygen-1		
field gradient					
$q(yy)$ (au)	1.1255	0.3516	1.1302	0.8781	0.4789
$q(zz)$ (au)	−0.3590	−2.5815	−0.6424	−1.7568	−2.2116
$\theta(zz)$ (deg)	0.0	29.5	43.3	31.6	30.1
anisotropic hyperfine					
$A(yy)$ (au)	−1.0788	−1.0272	−0.8149	0.1589	−0.2908
$A(zz)$ (au)	2.1355	−1.0387	1.6169	−0.0658	−0.3147
$\theta(zz)$ (deg)	51.6	16.5	4.4	0.8	20.3
			Oxygen-2		
field gradient					
$q(yy)$ (au)				1.9491	−2.7525
$q(zz)$ (au)				0.0734	0.4001
$\theta(zz)$ (deg)				66.8	62.2
anisotropic hyperfine					
$A(yy)$ (au)				5.7693	−1.7026
$A(zz)$ (au)				−1.9081	−1.6857
$\theta(zz)$ (deg)				65.9	57.7
			Hydrogen		
field gradient					
$q(yy)$ (au)	−0.1408	−0.1425	−0.1459	−0.1400	−0.1456
$q(zz)$ (au)	0.2855	0.2915	0.2777	0.2890	0.2953
$\sigma(zz)$ (deg)	0.0	0.0	0.0	0.6	0.4
anisotropic hyperfine					
$A(yy)$ (au)	0.0021	0.0051	−0.0183	−0.0098	−0.0100
$A(zz)$ (au)	0.0138	0.0087	0.0357	0.0268	0.0229
$\theta(zz)$ (deg)	0.0	0.0	0.0	0.0	39.0
isotropic hyperfine[c]					
a (au)	−0.0014	0.0004	0.1167	0.0111	−0.0003

[a] The z axis is parallel to the CH bond. D = debye. [b] The $(3y^2 - r^2/r^5)$ and $(3z^2 - r^2/r^2)$ components and the rotation angle between the molecule fixed z axis (oriented along the CH bond) and the principal electric or magnetic z axis are reported. [c] To convert the isotropic hyperfine constants from atomic units to gauss, at the hydrogen nucleus, multiply by 1594.9; to convert to megahertz multiply by 4469.5. To convert O^{17} anisotropic hyperfine values from au's to G, multiply by −25.82; to convert to MHz, multiply by −72.36.

to be explicitly included in the CI. This gives what we shall refer to as the estimated singles, doubles, quadruples CI (SDQ-CI) result. Ideally the estimated SDQ-CI energy should be the full CI energy and hence should be insensitive to addition or deletion of configurations near the threshold. The sensitivity of this estimated energy for $^2B_2$ is displayed in Table III. Addition to the reference wave function of more configurations with still smaller CI expansion coefficients would not appear to be justified. The uncertainty in the energy differences from this procedure is believed to be 1 kcal/mol, which is comparable with the likely error inherent in this basis set. The SDQ-CI energies for various states at the optimal SVP MCSCF geometries are given in Table IV. The actual sizes of the Hamiltonian matrices which were diagonalized ranged from 16 to 20 000 spin-adapted configurations.

Trends in the relative energies along the sequence 3-21G MCSCF, SVP MCSCF, and DZP CI are displayed in Figure 7. The most pronounced difference between the 3-21G and SVP columns in this figure is the previously noted destabilization of the $^2A_2$ and $^2A''$ π radical wave functions by roughly 5 kcal/mol relative to those for σ radicals. The same change in basis set destabilizes the C_s form of the σ radical ($^2A'$) by 2.6 kcal/mol relative to the C_{2v} geometry ($^2B_2$). With the greater flexibility in the hydrogen basis set, the DZP CI column shows a decrease in the $^2B_2$–$^2A_1$ energy gap, presumably because of the improved ability to describe the long C–H bond of the $^2A_1$ state.

The DZP CI calculation finds the energy at the C_{2v} π state geometry ($^2A_2$) to be about 2.5 kcal/mol below the energy of the C_s geometry ($^2A''$). The MCSCF calculation, in spite of its size, was apparently still unable to account adequately for the different correlation effects at the symmetric and nonsymmetric geometries. Unlike the case in allyl, the π surface for HCO_2· is very flat over a large change in geometry, and spurious minima may easily be caused by small effects.

The CI calculation also reverses the MCSCF energy ordering on the σ surface between the $^2B_2$ and the $^2A'$ geometries. As in the π state, the strong symmetry breaking at the SCF level leads to very different correlation effects at the symmetric and nonsymmetric geometries, so that it is difficult to find their energy difference accurately. The energy difference between these geometries, again 2.5 kcal/mol in our best calculations, is barely within the resolution of these computations. Thus, the σ surface is also very flat over a large change in geometry, but it is probably monotonically downhill in energy from $^2A_1$ to $^2B_2$ along the pseudorotation valley that passes through geometries with $^2A'$ wave functions.

Values of selected properties obtained with the DZP basis set SD-CI wave function are listed in Table V. For these calculations,

(20) Davidson, E. R. In "The World of Quantum Chemistry"; Daudel, R., Pullman, B., Ed.; Reidel: Dordrecht, 1974.

somewhat smaller reference lists were used and all single excitations from the reference space CI were retained. The molecules lie in the yz plane with the z axis oriented along the CH bond. Electric field gradients and hyperfine coupling parameters are given in the principal axis systems.

Discussion

EPR work by McBride and Merrill on the related benzoyloxyl radical, $C_6H_5CO_2$·, argues in favor of a $^2B_2$ ground state with equal C–O bond lengths. Their reported spin properties are generally in good agreement with our theoretical results for $^2B_2$ formyloxyl in Table V. The 52° angle between the two-fold rotation axis of the molecule and the local magnetic axis on oxygen, calculated at the CI level, is in excellent accord with their experimental result. The computed anistropic hyperfine parameters for ^{13}C are all somewhat too small in absolute magnitude, compared with the experimental values. For instance, converting the $^2B_2$ entries in Table V to gauss gives −3.29, 2.87, and 0.41 in the local x, y, and z directions, compared to −3.86, 3.08, and 0.78 obtained experimentally for benzyloxyl. The calculated ^{17}O anisotropic hyperfine splittings in gauss are 27.3, 27.8, and −55.1, which are all larger than those (19, 22, and −40) measured experimentally for benzoyloxyl.

The spin properties reported for benzoyloxyl by McBride and Merrill suggest a $^2B_2$ ground state for this radical, in agreement with our DZP SDQ-CI calculations on formyloxyl. Nevertheless, with a surface as flat as that which we compute for formlyloxyl, a phenyl substituent effect on the equilibrium geometry observed for benzoyloxyl should be considered.

Whether $^2B_2$ is a minimum or a transition state, connecting two A′ minima with unequal bond lengths, depends critically on the vertical energy separation of the $^2A_1$ state that can be mixed with $^2B_2$ by asymmetric distortion of the CO bond lengths. Since these two states differ in the occupancy of an MO ($6a_1$ in formyloxyl) that has appreciable density on the substituent group in acyloxyl radicals ($R–CO_2$·), a substituent effect on the preferred geometry of the lowest σ state seems possible.

Because calculations on benzoyloxyl of the same quality as those we carried out on formyloxyl were out of the question for us, we investigated the occurrence of a σ substutuent effect by comparing the $^2B_2$–$^2A_1$ energy difference in the two radicals. Calculations were performed at the RHF level with the Dunning [3s,2p/2s] basis set. The optimal geometry in $^2B_2$ of formyloxyl was used for the OCO portion of both radicals, and a standard benzene geometry was assumed for the phenyl group in benzoyloxyl. Figure 8 shows the singly occupied b_2 orbital in the $^2B_2$ state of benzoyloxyl, along with some geometry parameters.

At the RHF level of theory the computed $^2B_2$–$^2A_1$ energy difference is 33.6 kcal/mol compared to 31.4 kcal/mol in formyloxyl. The larger energy difference found in benzyloxyl would tend to favor a C_{2v} ground state more in this radical than in formyloxyl. However, the near identity of these two numbers provides no evidence of the operation of a significant σ substituent effect. Thus, the finding of a $^2B_2$ ground state for benzoyloxyl furnishes experimental support for our prediction of the same C_{2v} σ ground state for formyloxyl.

Acknowledgment. The authors thank the National Science Foundation for partial support of this research.

Registry No. HCO_2, 16499-21-1.

Flash-EXAFS for Structural Analysis of Transient Species: Rapidly Melting Aluminum

H. M. Epstein,* R. E. Schwerzel,* P. J. Mallozzi, and B. E. Campbell

Contribution from Battelle Columbus Laboratories, Columbus, Ohio 43201.
Received January 19, 1982

Abstract: Extended X-ray absorption fine structure (EXAFS) spectra of solid and flash-melted Al films have been measured simultaneously with a single nanosecond pulse of X-rays emitted from a laser-produced plasma. The results constitute the direct observation of a degree of local order in rapidly melting Al. This "flash-EXAFS" technique is thus demonstrated to be useful for the study of dynamic structural changes on the nanosecond time scale.

The extended X-ray absorption fine structure (EXAFS) technique has become recognized in recent years as a versatile tool for studying the structure of materials at the atomic level. EXAFS can provide information about the identities and spatial arrangement of the atoms in any type of solid, liquid, or gas, even those composed of highly complex molecules. In the EXAFS technique, the X-ray absorption coefficient of a material is measured as a function of energy from the K edge or L edge of a specific element in the material to as far as 1000 eV above the edge.[1,2] The absorption of X-rays by the element is accompanied by the ejection of photoelectrons, which can be scattered from neighboring atoms. Backscattering of these photoelectrons from atoms in the immediate vicinity of the absorbing atom gives rise to a periodic "wiggle" structure in the X-ray absorption spectrum.[1-4] By analyzing this wiggle structure above the absorption edge of a particular element, one can obtain information about the spatial arrangement of atoms in the immediate vicinity of the absorbing species. Since only the nearby atoms are involved, long-range order is not required; therefore, the EXAFS technique can be applied to the study of a broad class of materials, including liquids, gases, and amorphous or crystalline solids.

Previous work in our laboratories has indicated that laser-produced plasmas should be nearly ideal X-ray sources for fast EXAFS studies of transient structural phenomena and has resulted in the first experimental demonstration of the feasibility of performing EXAFS measurements with laser-produced X-rays.[5-7]

(1) (a) Sayers, D. E.; Lytle, F. W.; Stern, E. A. *Adv. X-ray Anal.* **1970**, *13*, 248. (b) Lytle, F. W.; Sayers, D. E.; Stern, E. A. *Phys. Rev. B: Solid State* **1975**, *11*, 4825. (c) Stern, E. A.; Sayer, D. E.; Lytle, F. W. *Ibid.* **1975**, 11, 4836.

(2) (a) Eisenberger, P.; Kincaid, B. M. *Science (Washington D.C.)* **1978**, *200*, 1441. (b) Cramer, S. P.; Eccles, T. K.; Kutzler, F.; Hodgson, K. O.; Doniach, S. *J. Am. Chem. Soc.* **1976**, *95*, 8059. (c) Cramer, S. P.; Hodgson, K. O. *Prog. Inorg. Chem.* **1979**, *25*, 1.

(3) (a) Kronig, R. de L. *Z. Phys.*, **1931**, *70*, 317; **1932**, *75*, 191; **1932**, *75*, 468. (b) Peterson, H. *Ibid.* **1936**, *98*, 569.

(4) (a) Ashley, C. A.; Doniach, S. *Phys. Rev. B: Solid State* **1975**, *11*, 1279. (b) Lee, P. A.; Pendry, J. B. *Ibid.* **1975**, *11*, 2795.

(5) (a) Mallozzi, P. J.; Epstein, H. M.; Jung, R. G.; Applebaum, D. C.; Fairand, B. P.; Gallagher, W. J. In "Fundamental and Applied Laser Physics", Esfahan Symposium; Feld, M. S., Javan, A., Kurnit, N. A., Eds.; Wiley-Interscience: New York, 1973; pp 165–220. (b) Mallozzi, P. J.; Epstein, H. M.; Schwerzel, R. E. *Adv. X-ray Anal.* **1978**, *22*, 267.

0002-7863/83/1505-1466$01.50/0